Fabrication and electromechanical performance of carbon nanotube based conductive membrane and its application in real-time multimode strain detection in composites

Yumna Qureshi, Mostapha Tarfaoui, Khalid Lafdi

Fabrication and Electromechanical Performance of Carbon Nanotube Based Conductive Membrane and Its Application in Real-Time Multimode Strain Detection in Composites

Yumna Qureshi* [(a)], Mostapha Tarfaoui*[(a)], Khalid Lafdi[(b,c)]
(a) ENSTA Bretagne, IRDL - UMR CNRS 6027, F-29200 Brest, France.
(b) University of Dayton, Nanomaterials Laboratory, Dayton, OH 45469-0168, United States
(c) Department of Mechanical and Construction Engineering, Northumbria University, Newcastle upon Tyne, UK

Abstract: In this study, a flexible conductive membrane (CM) consisting of a network of carbon nanotubes is produced and the electromechanical behavior of this CM was studied experimentally and the gauge factor (GF) of CM was in the 8-8.25 range. Then, a multi-mode strain detection is carried out in composites using this CM sensor. The CM is embedded gradually at directions i.e. 0°,+45°,90°,-45° between the plies for real-time/in-situ strain monitoring. The composite specimens are then cut in star profile and then tested under tensile and bending cyclic loading. There is a good reproducibility in the results and the mechanical response of composite correlated perfectly with the electrical resistance of the CM sensor however, a sensor in each position showed distinct behavior. The results established that the CM sensor exhibited good potential as a flexible strain sensor for in-situ monitoring of composites and can provide detection over a large section and unapproachable locations.

Keywords: Carbon nanotubes; conductive membrane; electromechanical performance; composites; real-time strain monitoring; multi-mode detection

Corresponding author: yumna.qureshi@ensta-bretagne.org, mostapha.tarfaoui@ensta-bretagne.fr

1. Introduction

Application of structural composites in the field of infrastructure, energy, aerospace, and the automobile has been increasing rapidly and these structures often experience a variety of conditions such as impact, bending, elongation, shock loading, or environmental effects [1]–[4]. The detection of local damage such as delamination, interlaminar failure, matrix softening, and matrix cracking in composites is often difficult to detect before the performance of the materials has been seriously compromised [5]–[7]. Non-destructive techniques (NDT) such as ultrasonic detection, x-rays, etc. can detect local damage, however, they often require disassembly of the structure for inspection and they are not able to detect damage instantaneously. Acoustic emission is often used for real-time monitoring of the failure in structures but, interpretation of the data is a complex process and mostly qualitative. So, it is important to discover novel methods for monitoring the deformation of the structure in real-time, and structural health monitoring (SHM) is a renowned and extensively used system to study the behavior of the structure in real-time to guarantee their reliability and safety [8]–[12]. Currently used SHM techniques include fiber optic sensors, piezoelectric or piezoresistive sensors, strain gauges, and accelerometers to monitor the mechanical deformation, vibrations, or other parameters of the structure during the operation [13]–[23]. However, most of these techniques can detect damage only near its location therefore, they must be placed near the critical zones on the structure. To counter this, sensor network systems had also been used to triangulate the location of the damage using Lamb wave propagation, but the cost, size, and weight of such a system limit their use in addition to their complex data analysis and processing [24]. The piezoresistive nature of carbon fiber reinforced composites has been studied as a self-sensing system to some extent but because of the electrically conductive nature of carbon fibers, this method does not apply to large structures due to their size and complexity of the design [25]–[27].

Numerous studies have focused on piezoresistive polymers made by dispersing nanofillers such as carbon nanotubes (CNTs) into the filaments of fibers or in the polymer matrix to increase the overall conductance of the structure were also considered as a possible solution of real-time strain monitoring [28]–[37]. In addition, a conductive polymer in the form of a thin-film, ribbon, thread, or any other desired shape can be formed using CNTs for sensing applications [32][38]. CNTs have been considered exceptional material since their discovery because of their high aspect ratio, electrical conductivity, and excellent mechanical and thermal properties [39]. Fibers consisting of CNTs have been used in SHM of damage in structures due to their excellent mechanical behavior, flexibility, and deformation sensitivity [40]–[43]. To have excellent conductivity, CNTs are usually implemented in well-aligned free-standing or a conductive membrane (sheet) of randomly oriented CNTs named as bucky paper [44]–[50]. However, several studies showed that oriented and CNTs grown on a specific substrate required critical control on the fabrication process to ensure better dimension and spacing of CNTs [51]–[53]. Therefore, the fabrication of bucky paper/ conductive membrane was inspired by the

simplicity of the fabrication process and ease to use especially on a large scale. The conductive membrane is a laminar structure of randomly oriented CNTs held together by the van der Waals forces. This conductive membrane/ bucky paper had been utilized to developed chemical sensors, actuators, supercapacitors, and flexible fibers [54]–[58]. However, their application in real-time monitoring of mechanical deformation of structures under different loading conditions is still underdeveloped or limited.

In this experimental investigation, the real-time strain detecting ability of the CNTs based conductive membrane (CM) was examined under tensile and flexural loading. A CM sensor with good flexibility was developed through chemical vapor deposition (CVD) of randomly oriented CNTs in the form of a membrane on a quartz wafer with a thickness of 120 µm. Then, the sensitivity of the CM to the applied strain was calculated experimentally by gauge factor (GF) calculation using a standalone sensor. Afterward, the general electromechanical behavior of CM was examined up to fracture to validate the response of the CM sensor under large strain application or during any damage that was vital to comprehend its use in high strain applications. Afterward, this CM sensor was positioned in 0°, +45°, 90°, -45° directions through the plies gradually in a glass fiber reinforced polymer (GFRP) composites, and the composite specimens were tested under tensile and flexural cyclic loadings. The results showed that the CM sensor did not only detected the strain under both loadings but also the intensity of the signal measured the amount of deformation. Moreover, the results demonstrated that the position and direction of the sensor play a vital role in the detection of strain by the sensor.

2. Sample Fabrication

2.1. Conductive membrane (CM) sensor

A conductive membrane (CM) was fabricated using a chemical vapor deposition (CVD) method by growing CNTs on a quartz crystal, Figure 1. This process consisted of two steps in which the first catalyst was prepared and then CNTs were synthesized. The wafer, cut in specific dimensions, was first heated in an oven at 500 °C for 10 mins and then after cooling down to room temperature, it was dipped in the catalyst solution consisting of ethanol and Fe-Mo in a mol ratio of 10:1. Afterward, the Fe catalyst deposited on the wafer was reduced by placing it in a quartz tube in a tube furnace and heating at 800 °C in argon and hydrogen gas. Lastly, in the presence of ethylene gas, the substrate was subjected to a carbon source. This ethylene gas triggered the breakdown of carbon and led to the synthesis and deposition of CNTs on the wafer. After fabrication, the sample was pressed between two parallel plates in successive steps to ensure denser film in the form of a membrane of 120 µm thickness and separate it from the wafer. We managed to produce CNTs with a length of about 200 µm with a diameter of about 10 nm. Figure 2 demonstrates the SEM characterization of the CM sensor consisting of a dense network of CNTs. It’s a laminar structure of randomly oriented CNTs held together by the van der Waals forces.

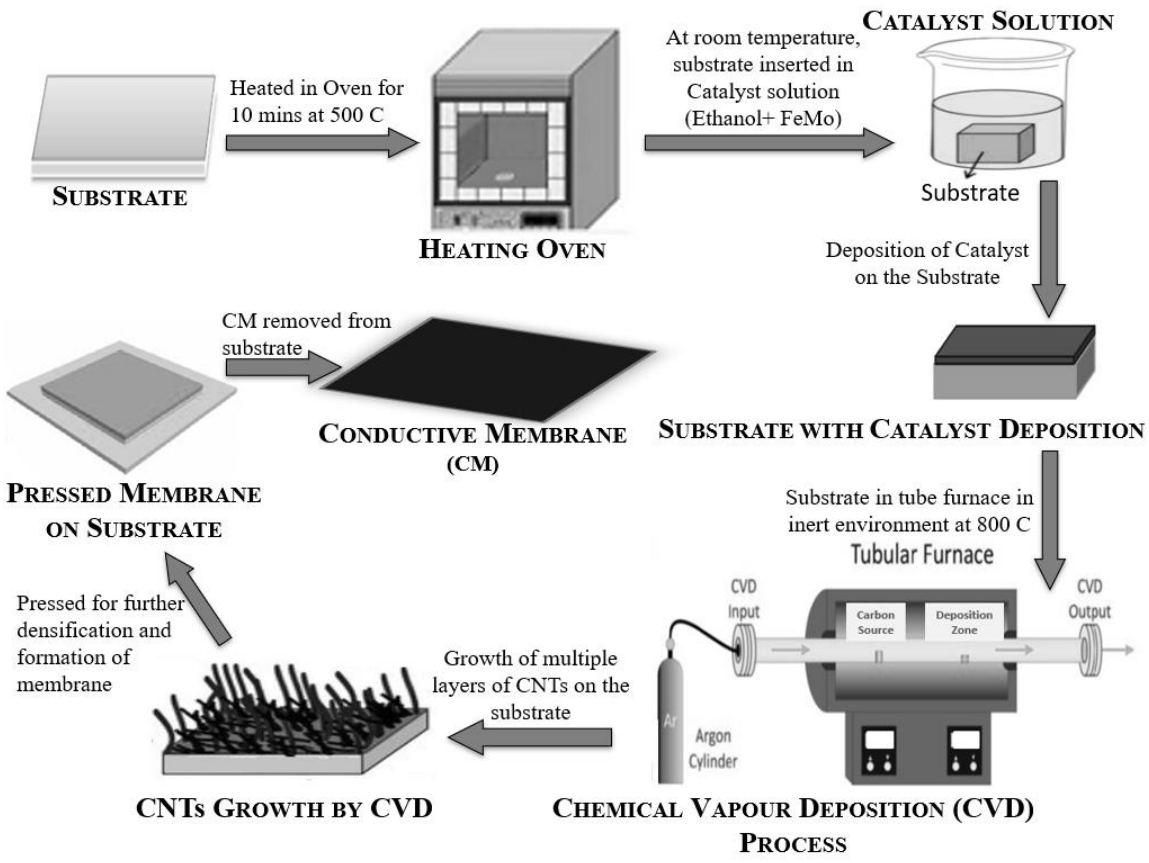

Figure 1: Fabrication Process of CM Sensor

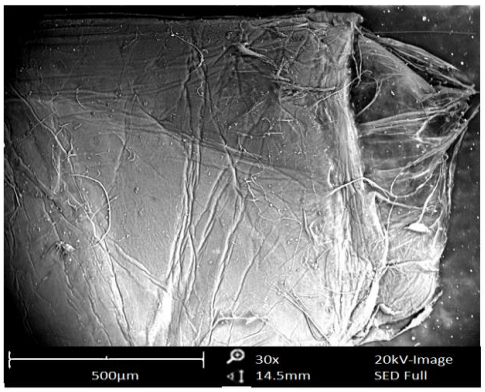

(a)

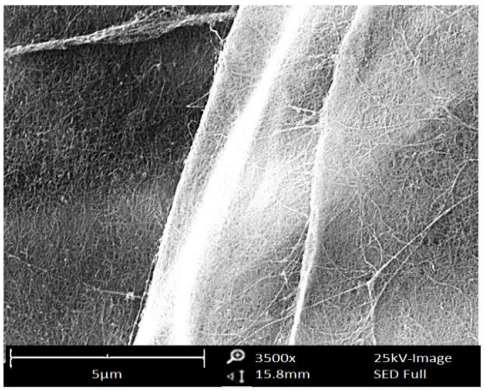

(b)

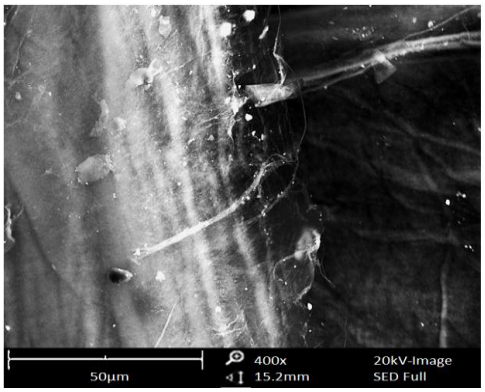

(c)

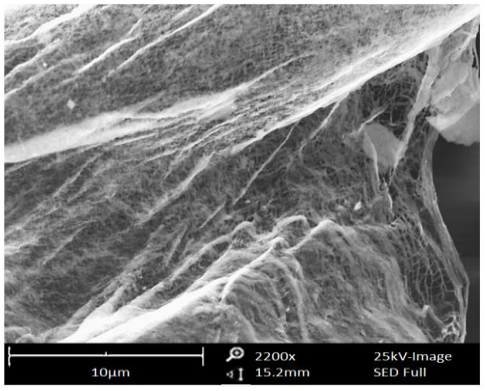

(d)

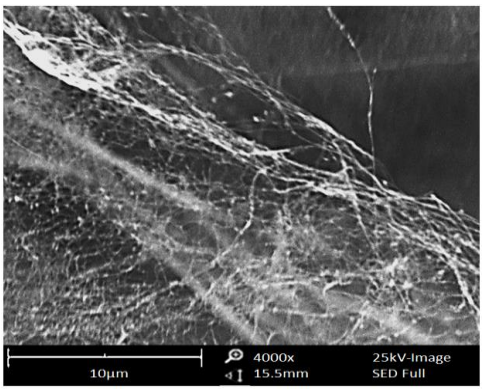

(e)

Figure 2: SEM images of CM sensor. (a) CM sensor (b) magnified image on the surface of the CM sensor to demonstrate the network of CNTs (c) SEM at lower magnification on the edge of the membrane (d)-(e) magnified SEM image on the edge of the single layer of membrane to show the network of CNTs in forms of threads of fabric.

2.2. Composite samples embedded with CM sensor

The process of integrating CM sensors in a composite specimen for in-situ strain monitoring required electrical isolation of the CM sensor in each position and direction. That is why composite specimens were prepared using chopped glass fiber plies because of their high electrical resistance and non-conductivity and it also ensured the isotropic nature of the composite sample. Five plies of chopped glass fiber mat were used in a single composite specimen and each CM sensor was placed in its respective directions i.e. sensor A in 0°, sensor B in 45°, sensor C in 90°, and sensor D in -45° and were separated by each ply. Then, the Epon 862 resin and w30 hardener mixture in a 1:4 ratio was added to the mold and total incorporation of the CM sensor in an individual position was accomplished. Then, the sample was left at room temperature for 2 days for curing and the sensor in each position was visible in all cured specimens. Then, each composite plate was cut into a star shape and the individual leg indicated the position and direction of CM, Figure 3a. The thickness of the composite specimen was kept as 5 mm and the width and length of the individual leg of the star sample were kept at a standard measurement of 25 mm and 200 mm respectively, Figure 3b. Schematic illustration of the composite star sample integrated with CM sensor showed that sensor in each leg was represented by sensors A, B, C, and D according to their reference direction and the position of each sensor within the plies of the sample.

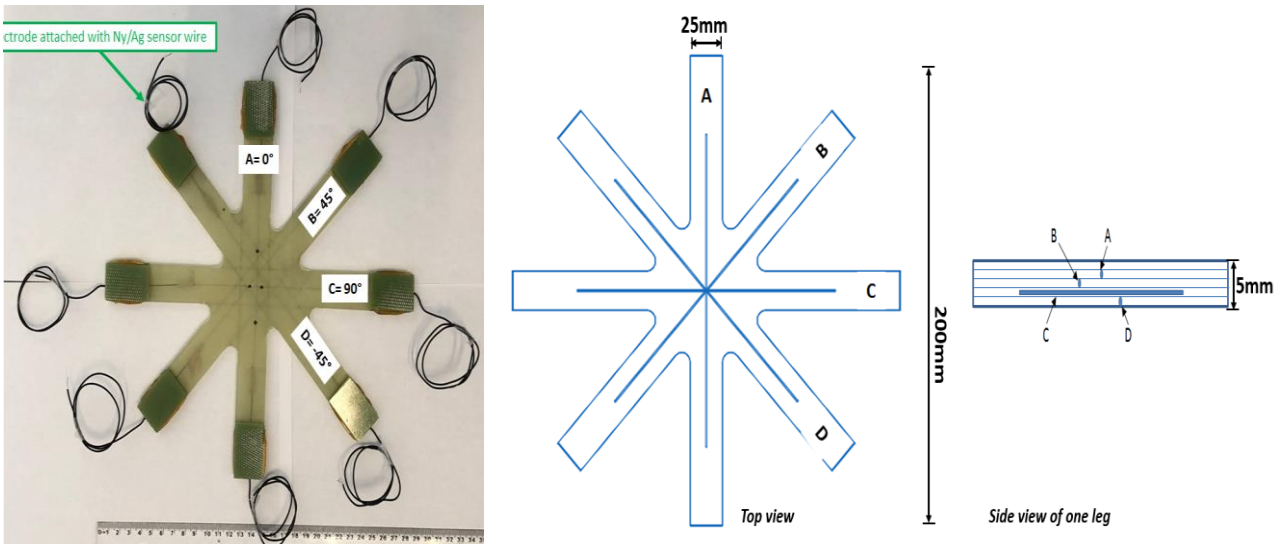

(a) *(b)*

Figure 3: (a) Composite sample integrated with CM sensor and sensors are visible in each position as the samples became transparent after the curing method. (b) Geometric specifications of the composite specimen and schematic illustration of the direction and position (section view) of the CM sensor.

3. Experimentation

3.1. Experimentation of standalone CM sensor for GF calculation

CM sensor was tested under tensile load as a standalone sensor of 72 mm length and 0.5 mm width using the INSTRON-50 apparatus, Figure 4a. The data acquisition system was attached through electrodes at both ends of the CM to simultaneously record the variation in the electrical resistance with the applied strain and calculate its gauge factor (GF). CM sensor was very delicate to handle, and because of its fragility, it was quite challenging to place the sample between the fixtures during the standalone test. The sample was placed in the machine using paper support as it was difficult to place the delicate CM alone between the fixture of the machine and before the start of the test, the paper frame was cut in the middle to not affect the mechanical response of the CM sensor during the test, Figure 4a. In addition, all the electrical contacts were isolated from any metallic part of the machine using insulation tape to ensure that the electrical signal of the CM sensor could not be influenced. The CM sensor was placed unstrained between the fixture before the test and no slippage occurred between the electrode and sensor connection during the test, Figure 4b. Three successful tests were conducted with CM sensor up to fracture to comprehend its electrical behavior with the variation in mechanical performance for high strain applications. The sensor was applied with tensile strain at the low strain rate of 2 mm min^{-1} and the results showed repeatability in their mechanical and electrical response which will be discussed in detail in the next section.

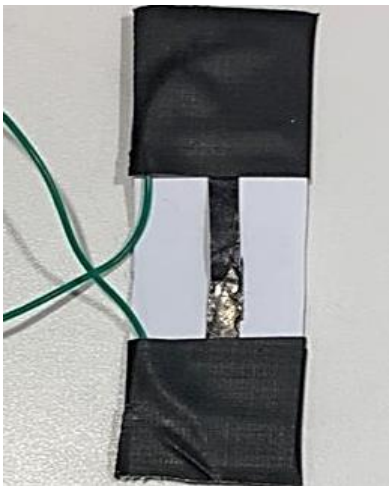

Figure 4: Preparation of CM sensor for standalone experimental test for the GF calculation. Set of papers are used as a support and electrode is attached on each end

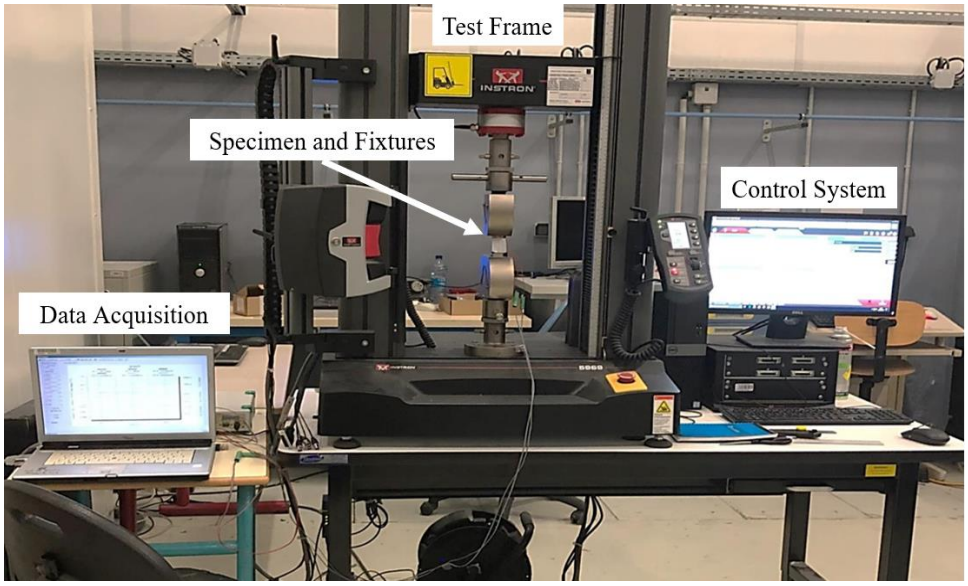

(a) Experimental Setup consisting of data acquisition, INSTRON-50 machine, control system and fixtures, and specimen in respective tests.

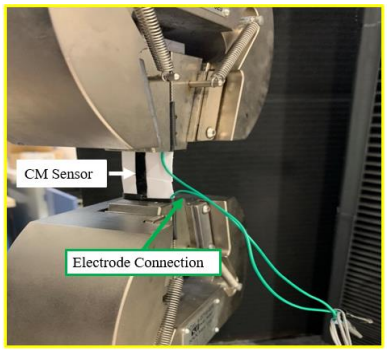

(b) Standalone CM sensor for GF calculation

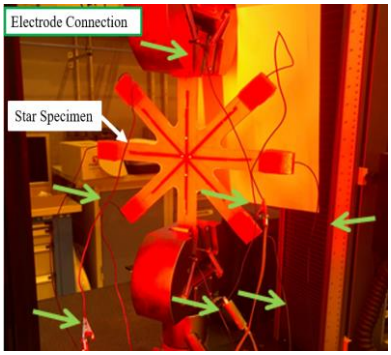

(c) Tensile test

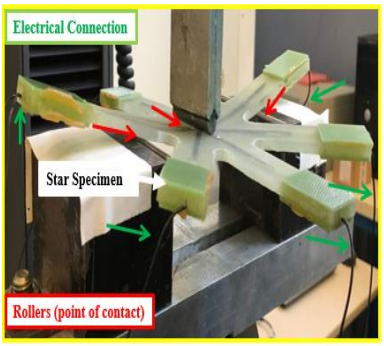

(d) Bending test

Figure 5: Experimental Testing Setups

3.2.Experimental testing of composite integrated with CM sensor

Composite specimens integrated with CM sensors in different direction and position was tested using INSTRON-50 and data acquisition system was attached to each sensor using electrodes for real-time monitoring of strain deformation. INSTRON-50 recorded the mechanical performance of the composite sample and the data acquisition system simultaneously recorded the response of each CM sensor. Two sets of tests were performed on the composite star specimens. The first set of tests included the study of three composite specimens under tensile cyclic loading and the second test was included the testing of three-star specimens under cyclic bending to comprehend the real-time monitoring behavior of the CM sensor in detail, Figure 4c-4d. Moreover, the shape of the specimen made it easier to place it between the fixtures during the tensile cyclic loading but the placement of the specimen between the rollers of the flexural cyclic test was a bit difficult. That is why the strain rate for the tensile test was kept at 5 mm min^{-1} applied up to 15 kN and for the flexural test, it was kept 2 mm/min applied up to 2 kN to ensure no permanent deformation in the samples. All tests were performed for 10 cycles and it must be noted that the range of strain rate in quasi-static tests is so low that it does not strain hardening in the mechanical behavior of the sample or any hysteresis in the electrical response of the sensor [59]. Each test presented that the CM sensor in each position and direction showed a distinct resistance profile in both sets of tests which will be discussed in detail in the next section.

4. Result discussions

4.1 Mechanical Behavior of CM sensor

The CM sensor displayed good mechanical behavior in terms of Young's modulus and yield strength which were about 1.119 +/- 0.024 GPa and 1.06 +/- 0.0256 MPa, respectively were +/- denotes the sample standard deviation, Figure 6a. Table 1 summarizes the mechanical behavior of the CM sensor, consisting of yield’s strength, Young's modulus, and fracture strain. In overall mechanical behavior, each sensor sample exhibited nonlinear (plastic) deformation before final fracture which specified that the membrane was quite flexible and might be applicable in high strain applications without compromising its mechanical performance, Figure 6b. The dense network of CNTs in the CM started to overcome the wander Vaal's forces when elongated and showed plastic deformation before the initiation of its breakage. Furthermore, it was observed that after plastic deformation, the damage initiation and propagation were not sudden, and the membrane was fractured gradually.

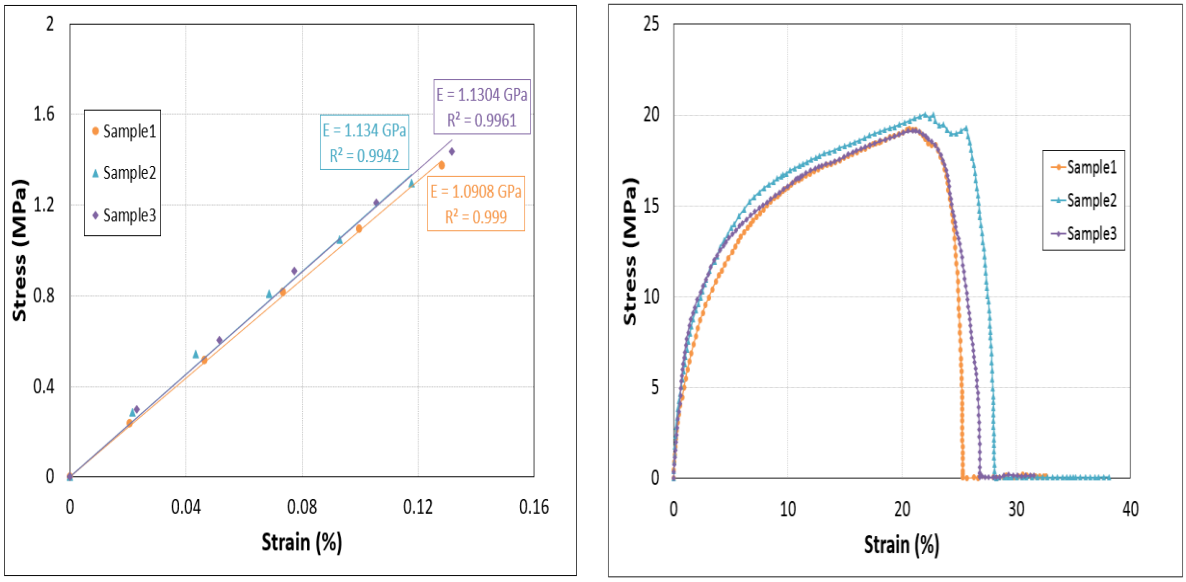

(a) Elastic Modulus *(b)Overall mechanical behavior*

Figure 6: Mechanical performance of CM sensor.

Table 1: Mechanical properties of CM sensor under tensile loading

	Elastic Modulus (GPa)	**Fracture Strain (%)**	**Yield Strength (MPa)**
Sample 1	1.09050	25.40	1.60
Sample2	1.13440	28.08	1.58
Sample3	1.13040	26.80	1.63
Average	1.11843	26.76	1.60
Standard deviation	0.0242735	1.3419	0.0256

4.2 Strain sensitivity calculation of CM sensor

The resistance of the CM sensor increased with the applied tensile strain showing a good correlation with its mechanical response, Figure 7a. The sensitivity of the CM sensor was demonstrated in terms of GF by comparing the variation of resistance with the amount of applied tensile strain and calculated by using equation (1).

$$G.F = \frac{(\triangle R/Ro)}{\varepsilon} \quad (1)$$

In this equation, $\triangle R/R_o$ is the ratio of change in resistance to the initial resistance, and ε is applied strain. Assuming the elastic limit is 2%, the GF in the elastic range was calculated to be 8.14 +/- 0.11, which almost 3 times higher than the metal strain gauges [42], Figure 7b. In previous studies, bucky paper consisting of dense network of CNTs showed almost 7 GF [30] and paper based CNTs strain sensor showed 7.5 GF [42]while CNTs based tablet showed GF up to 50 [29] because of being pressed between two plates under the pressure of ~ 200-300 MPa to ensure maximum densification, Figure 8. Furthermore, self-resistance of CNTs based nanocomposites and CNTs/polymer composite strain

sensors are also studied for strain monitoring applications however, their GF depends upon the weight % of CNTs used to overcome the threshold level [36]. All these sensors have complex and expensive fabrication processes and depend upon the tunneling effect which can affect the overall resistance of the sensor. Moreover, most of these sensors are studied under single applied load to detect deformation in simple structural models to their strain sensitivity and integrity. None of them were studied to quantify the deformation under cyclic load in different directions and position at multiple locations and most of them were externally attached to the structure for the monitoring of the strain. The comparative study confirmed that the CM sensor had a good strain sensitivity range and can be used for instantaneous strain monitoring of structures.

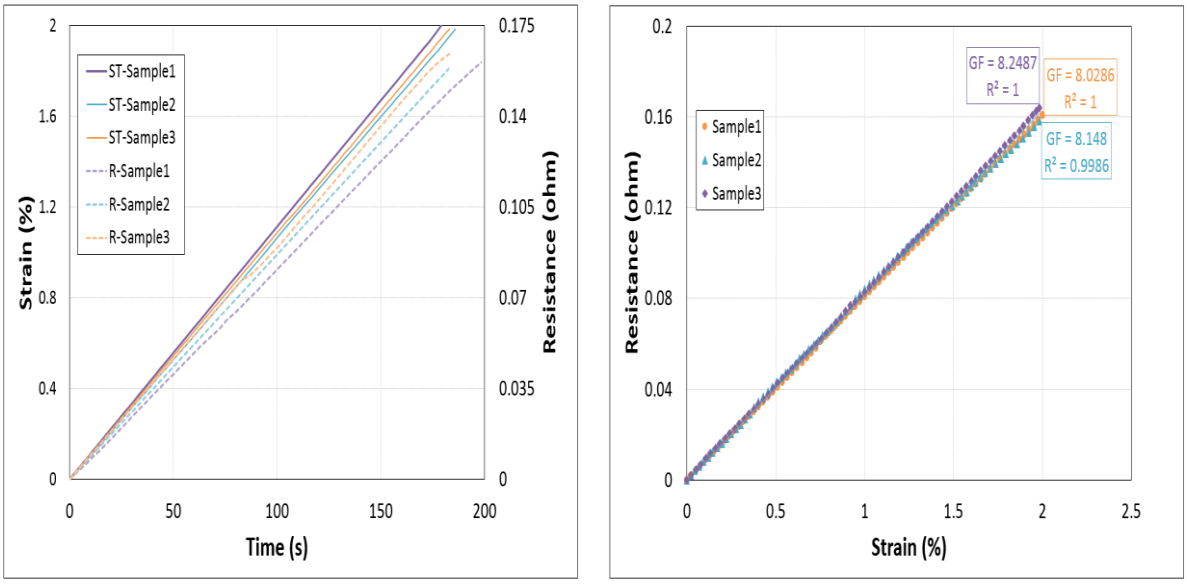

(a)Strain and resistance change in CM sensor during elongation

(b)GF calculation

Figure 7: Experimental behavior and calculation of the strain sensitivity of the CM membrane sensor

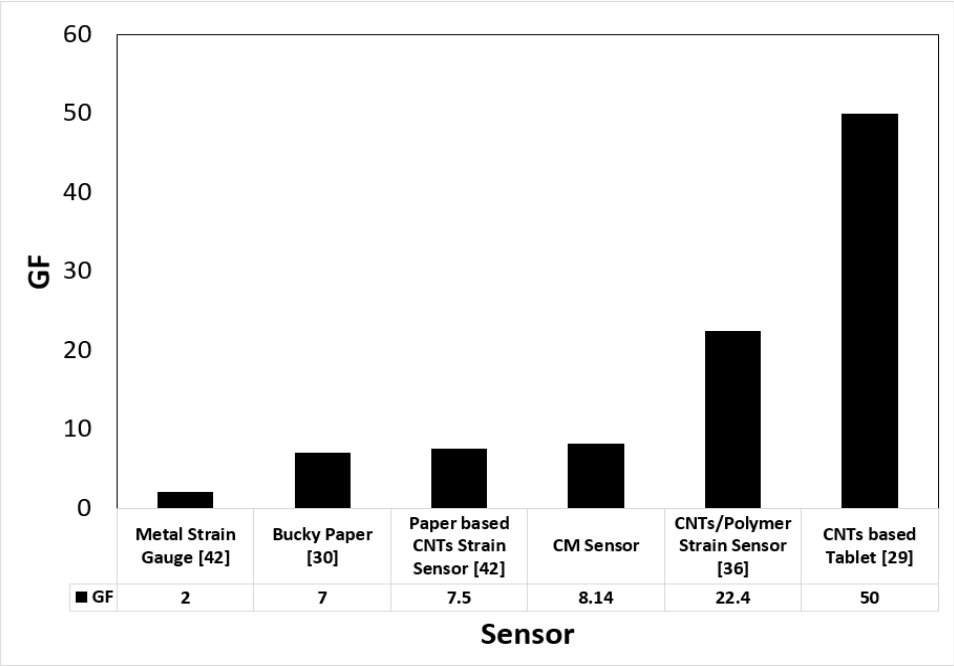

Figure 8: Comparative study of CM sensor with other CNT based sensor types

Each specimen of CM sensor presented good electrical behavior throughout the applied tensile strain, resistance changed gradually, and all samples displayed similar overall performance. The overall behavior of the CM sensor presented that, during elastic-plastic behavior the change in resistance was linear, and when the mechanical behavior of the sensor started to degrade there was a sudden increase in the resistance which reached maximum value upon fracture of the membrane, Figure 9. The change in resistance showed linear and directly proportional behavior with the applied strain during initial deformation of the sensor, equation (2)-(3).

$$\alpha = \frac{1}{\rho} \tag{2}$$

$$R = \frac{\rho L}{A} \tag{3}$$

where α is electrical conductivity, ρ is resistivity, L *is* length, A is the cross-sectional area, and R is resistance.

The CM sensor showed a gradual and linear change in resistance as the sensor started to experience deformation at the applied strain. The inset box showed that the sensor showed a detection signal even during elastic deformation and plastic deformation (after the yield point). The sudden increase in this behavior of resistance is after the achievement of maximum stress at around 23-24% yield because of the initiation of damage or facture in the membrane at the micro-scale. When the CM sensor showed a full fracture, the resistance achieved its maximum value of around 30-40% strain. Therefore, the sensor is not only able to damage initiation and fracture but also able to monitor the strain deformation

and can be used for high-strain monitoring applications. This confirmed its ability to use for real-time strain monitoring application during high strain deformation of structures.

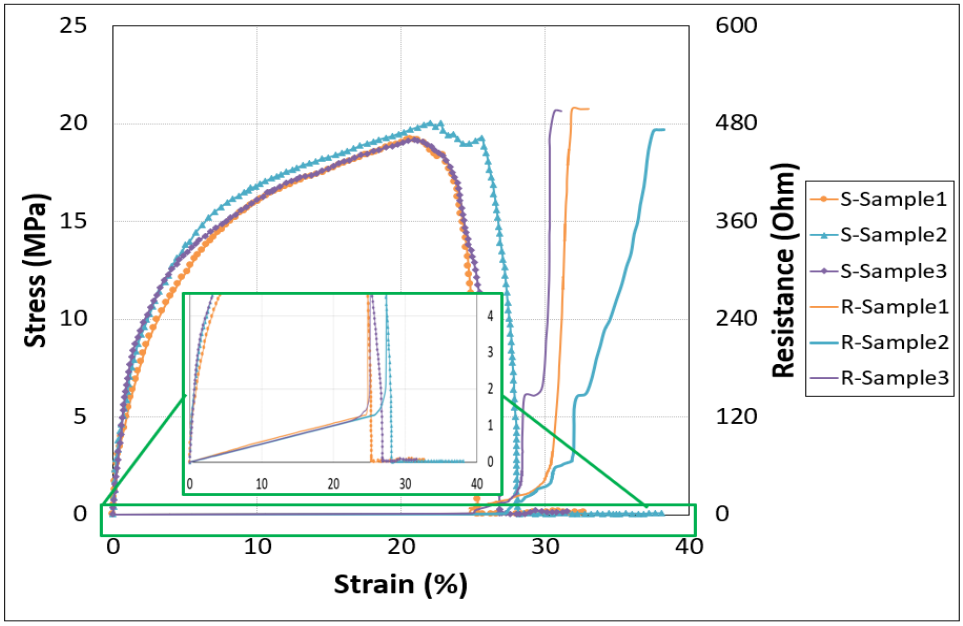

Figure 9: Overall electromechanical response of CM sensor specimens.

5 Real-time strain monitoring application of CM sensor

5.1 Strain monitoring in composites during cyclic tensile loading

First, it is important to understand the strain deformation of the composite under cyclic tensile loading to apprehend the strain detection by the CM sensor, Figure 10. One leg of the star specimen was fixed between the fixtures of the machine and the other legs were free. The loading axis was considered as the reference and the sensor place in this direction was at 0° and labeled as sensor A. When the specimen was loaded, tensile stresses were produced at 0° and compression stresses were produced in 90° i.e., transverse direction. In addition, it was understood that the combined effect of tensile and compression stresses is generated in oblique direction i.e., $\pm$45°. However, in test 1 and 2, samples were placed between the fixtures in such a manner that the leg of the star sample consisting of sensor A was along the loading axis i.e., in 0°, and in test 3 sample was placed in a way that the leg of the composite sample consisting of sensor C was along the loading axis i.e. in 0°, sensor A in 90° and sensor B & D interchanged their position, Figure 11. The step to interchange the positions of the CM sensor in test 3 was conducted to examine the load sensitivity of the CM sensor and it did not affect the comparison of the mechanical performance of the composite samples. Three composite specimens were tested successfully, and mechanical behavior was plotted as elastic modulus and overall initial stress-strain curve which showed good repeatability in the behavior, Figure 12. Results confirmed that the mechanical behavior of all composite samples was similar irrespective of the choice of the loaded leg, was isotropic because of the use of the chopped glass fiber mat, and the presence of CM sensor in

different directions and position did not affect the structure's integrity.

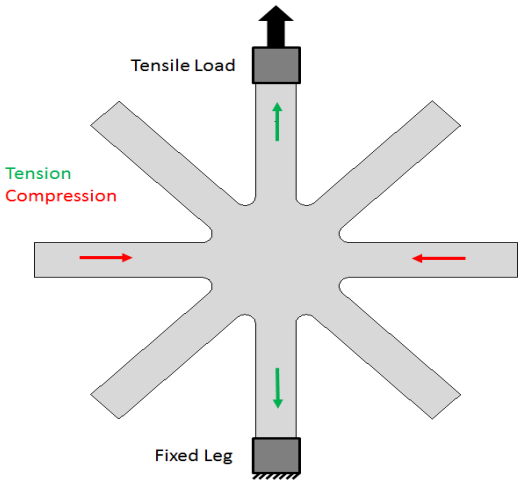

Figure 10: Deformation mechanism of the specimen during the applied tensile strain.

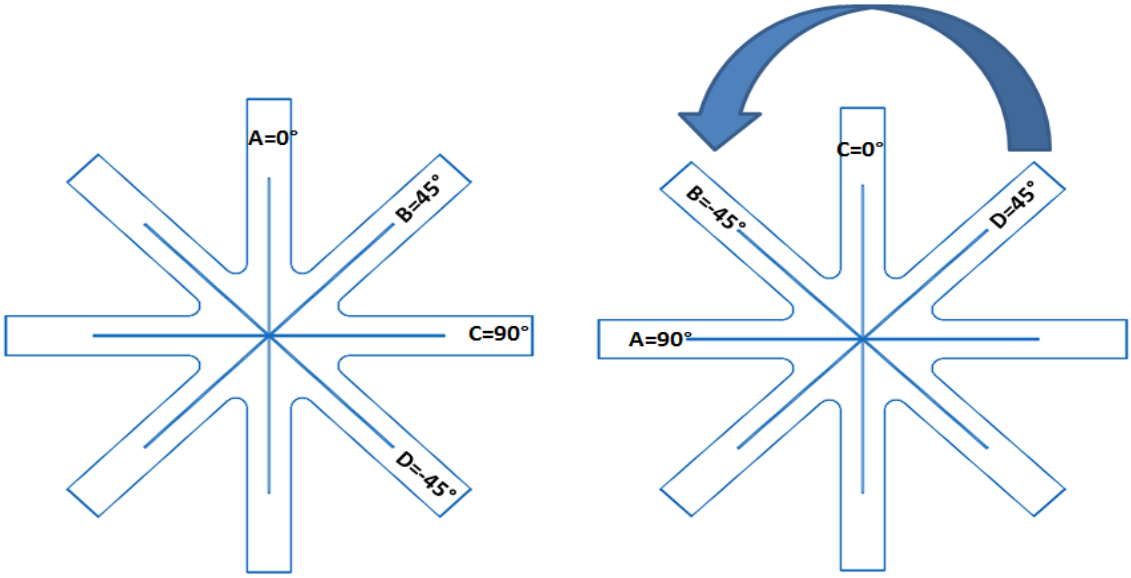

(a) Samples position in test 1 and 2 *(b) Sample position in test 3*

Figure 11: Placement of the composite sample between the fixture of the tensile machine

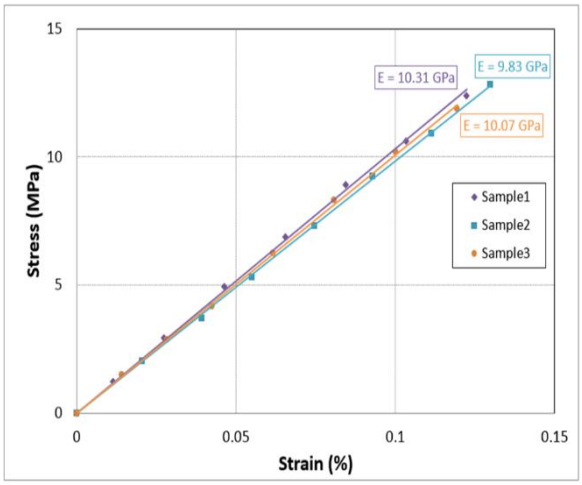

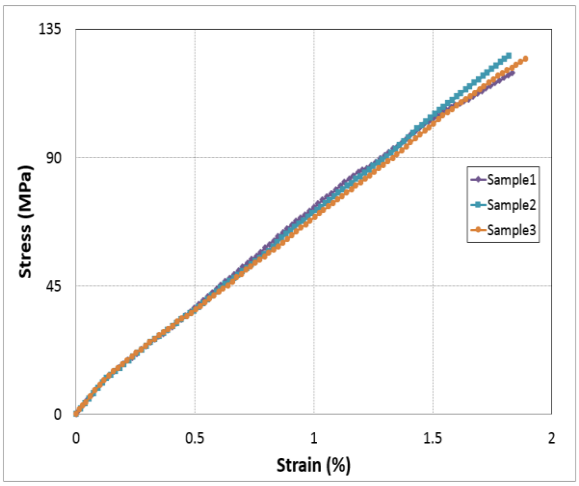

(a) Young's modulus *(b)* Overall initial stress-strain behavior

Figure 12: Mechanical performance of the composite star sample.

Flexible CM sensor displayed good electrical variation during the strain deformation of the composite specimen in all three experimental tests. The resistance of the CM sensor in each composite sample showed gradual change during each cycle of applied strain and showed similar behavior in each direction. However, the electrical resistance of the CM sensor within a single specimen showed different intensity in the change of the signal with the applied strain because of their specific direction i.e. 0°, ±45°, 90° regarding the loading axis. This showed that the CM sensor did not only monitor the strain but also showed the amount of strain-induced in each direction with respect to the applied load. Moreover, the consistency of the recorded signal during all 10 cycles showed the stability, durability, and integrity of the CM sensor.

- Tests 1 and 2 were performed to further confirmed the repeatability in the behavior of the CM sensor when produced in different batches. All the sensors A, B, C, and D presented variation in resistance according to the intensity of the deformation in their direction and correlated perfectly in both tests and each cycle, Figure 13. Furthermore, sensor A demonstrated the maximum change in its resistance when subjected to the cyclic loading that established the presence of maximum deformation of the sample in the loading direction because of the tensile elongation. Then, sensor B and D presented less variation in their resistance during the cyclic strain in comparison with sensor A because of their direction. Moreover, sensor place in B and D direction displayed an identical change in resistance which is because these two positions were the mirror of each other regarding the loading axis and they confirmed the isotropic nature of the material. CM sensor in position C showed minimum variation in the resistance due to its transverse direction with respect to the loading axis. This change was positive however, a negative change was expected because of the compressive strains, to justify the Poisson's effect under tensile loading [8], [10]–[12]. This positive change could be because of the complex interaction between the laminar stresses and the conduction behavior of the CNTs in the conductive membrane. One reason could be the fact that the curing process densified the arrangement of the CNT network in the layers of conductive membrane and additional compression could not cause a further reduction in the resistance of the CM sensor [59].
- Sample 3 was tested and compared with the results of Sample 1 to test the load sensitivity of the CM sensor, Figure 14. In test 3, sensor C recorded the maximum change in the resistance during the cyclic tensile load because of its position along the loaded axis and sensor A showed detection of minimum strain deformation because of its transverse position with respect to the loading axis. However, CM sensors placed in B and D showed an identical change in the signal because of their similar direction according to the loading axis in both tests 1 and 3 i.e. $\pm$45°.

Moreover, it was observed that the intensity of the change in signal of the CM sensor in a particular position was similar in both cases i.e. test 1 and 3 regardless of sensor label. For instance, sensor A in test 1 and sensor C in test 3 showed the almost equal intensity of the increase in resistance with the applied strain because of a similar position. Similar behavior was observed for the rest of the position which confirmed that the position of the sensor plays a key part in not only detecting the deformation but also identify the amount of strain produced in the respective direction. Thus, this confirms the sensitivity of the sensor is dependent on their location according to the loading direction, Figure 15.

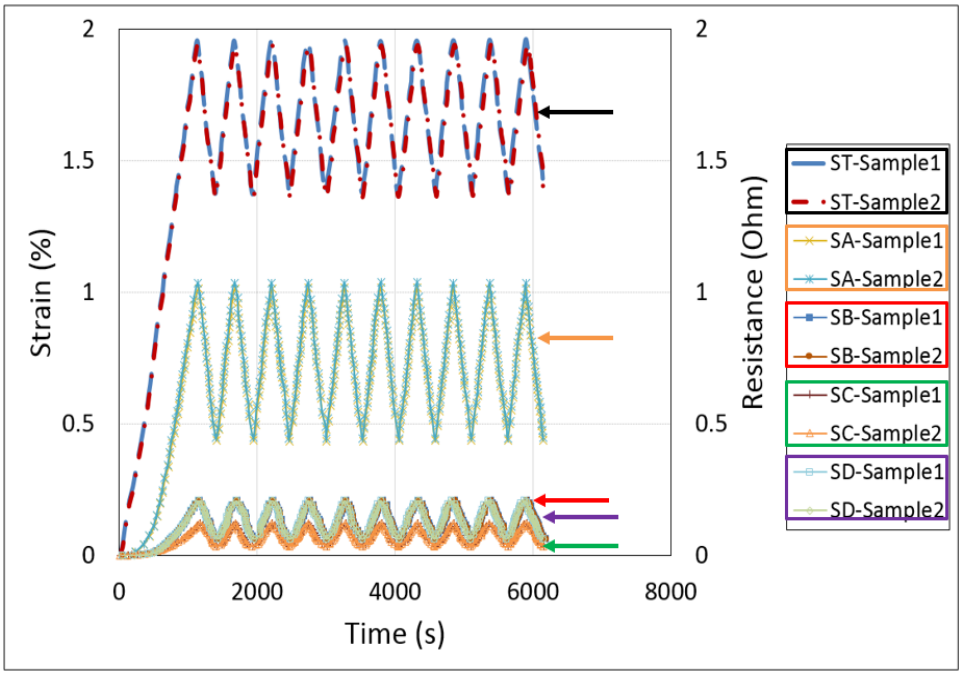

Figure 13: Real-time tensile strain monitoring in the composite by CM sensor and verification of the reproducibility of the test

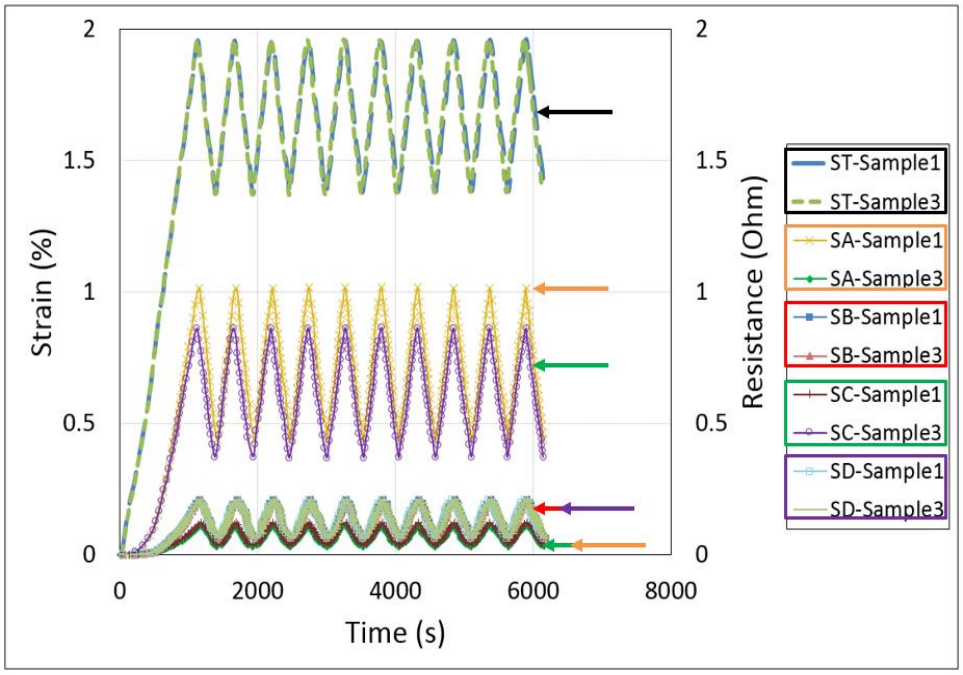

Figure 14: Comparison of real-time strain monitoring of composite star specimen by CM sensor during test 1 (when sensor A is placed in loading direction) and test 3 (when sensor C is placed in loading direction)

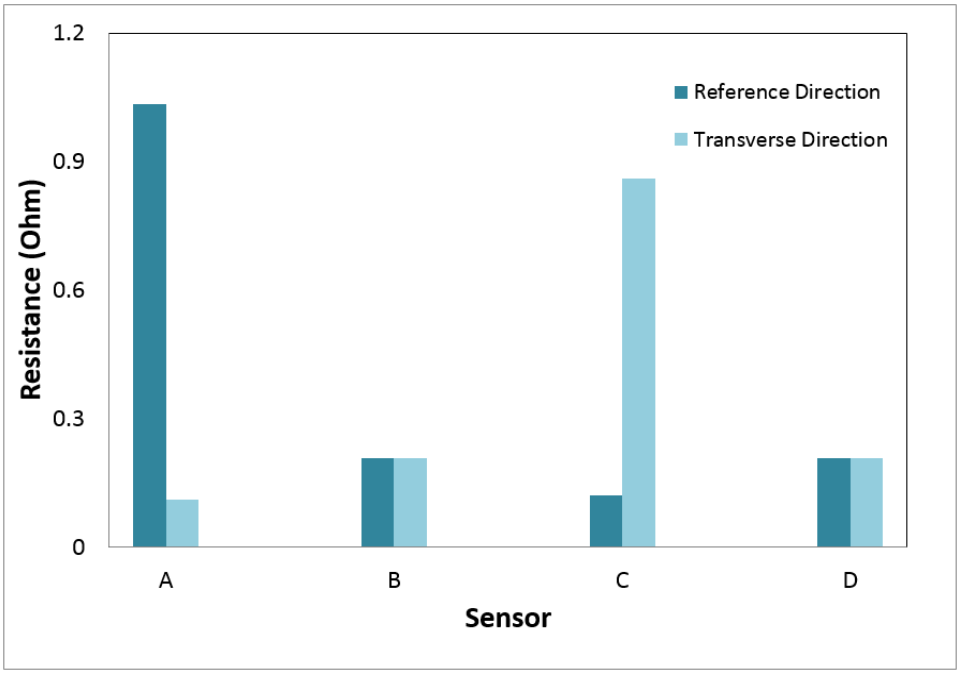

Figure 15: Effect of position and direction on the sensitivity of the CM sensor with respect to the applied load.

5.2 Strain monitoring behavior in composites during cyclic flexural loading

Like the tensile test, it is also significant to understand the strain of the composite sample during the three-point bend test to apprehend the response of the CM sensor during the detection of flexural strain. The Star specimen was placed in the machine for a three-point bend test in such a manner that one leg

of the star sample was loaded among three roller-fixtures in addition all other legs were free. The loaded leg was positioned on the two roller-fixtures on the bottom and the third upper roller-fixture was used to apply the force and deflection, Figure 16a. Moreover, it should be kept in mind that in all three tests, the star specimen was placed between the rollers such that sensor A was in the roller axis direction and sensor C was in the loaded leg i.e., within the span length. Once the sample was deflected during the three-point bend test, it was deformed within the span light and there were compressive strains (green arrows) at the upper surface because of the compressive force of the upper roller-fixture and tensile strain near the lower surface of the sample due to the tensile elongation (red arrows), Figure 16b. Then these tensile (from bottom) and compressive (from top) strains propagate through each ply which could result in sample failure.

Three samples were tested in such a manner that samples in tests 1 and 2 were placed between the rollers with sensor A in the topmost place within the roller axis (Case I) and sample in test 3 was placed between the roller with sensor D in the top position and sensor A in the lowest place (Case II) while sensor C was along the span length in both cases, Figure 17. This step was carried out to study the position sensitivity of the CM sensor and its capacity to sense strain deformation within the plies of the composite during flexural deflection. Mechanical behavior under flexural loading was calculated using equation (4)-(6) and results showed that inverting the positions of the sensors did not affect the mechanical performance of the composite with good reproducibility in the mechanical behavior, Figure 18. The flexural modulus on average was found to be 10.103 +/- 0.0737 GPa which shows excellent agreement with the tensile modulus and confirmed the uniform and consistent fabrication process. This further established that the presence of flexible CM sensors in distinct directions and positions did not affect the overall mechanical performance, structural integrity, and isotropic nature of the star specimen [8].

$$\sigma_f = \frac{3FL}{2bd^2} \tag{4}$$

$$\varepsilon_f = \frac{6Dd}{L^2} \tag{5}$$

$$E_f = \frac{L^3 m}{4bd^3} \tag{6}$$

where, σ_f is the flexural stress, ε_f is the flexural strain, E_f is the flexural modulus of elasticity, F is the load, L is the span length, b is the width, d is the thickness, D is the deflection, and m is the slope of the load-deflection graph.

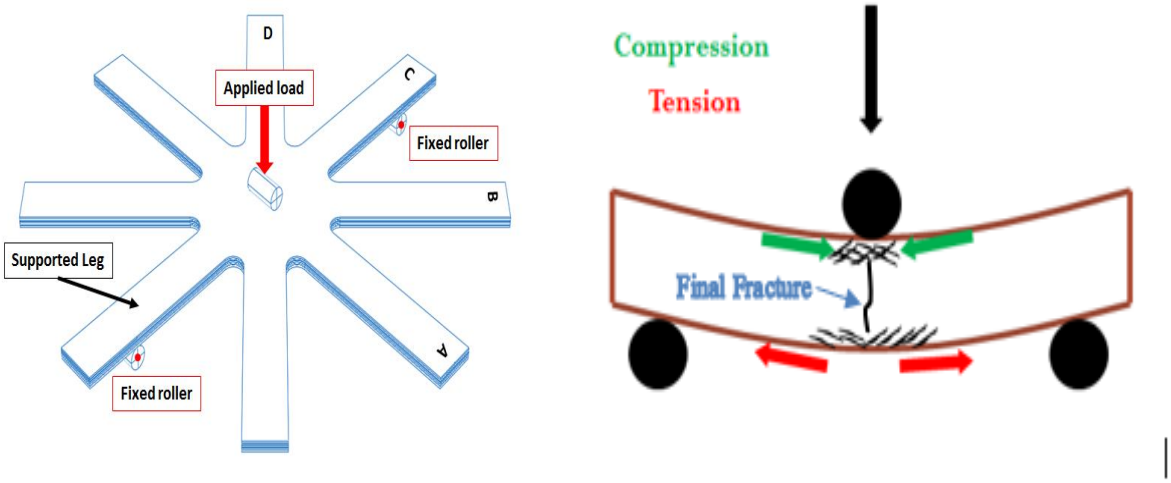

(a) Placement of the Specimen between the roller fixtures in the machine

(b) Deformation behavior of the specimen

Figure 16: Mechanical strain deformation of composite star sample during flexural loading.

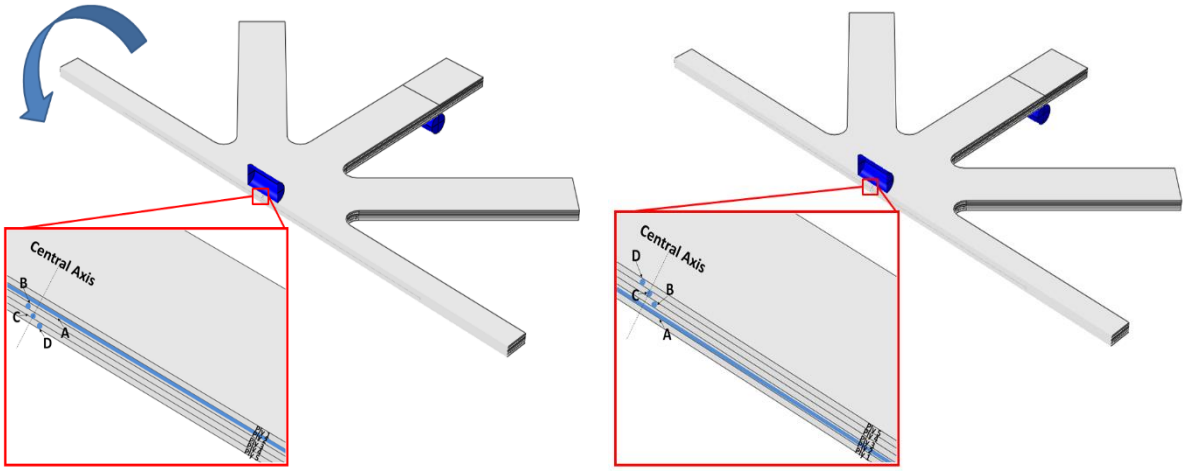

(a) Case I

(b)Case II

Figure 17: Placement of the star specimen between the three rollers fixtures for flexural bending: (a) Samples placed during test 1 and 2 when sensor A is in top position and sensor D is in lowest position (b) Sample placed during test 3 when sensor A is in the lowest position and sensor D is in top position. Sensor C is in the loaded leg during all three tests.

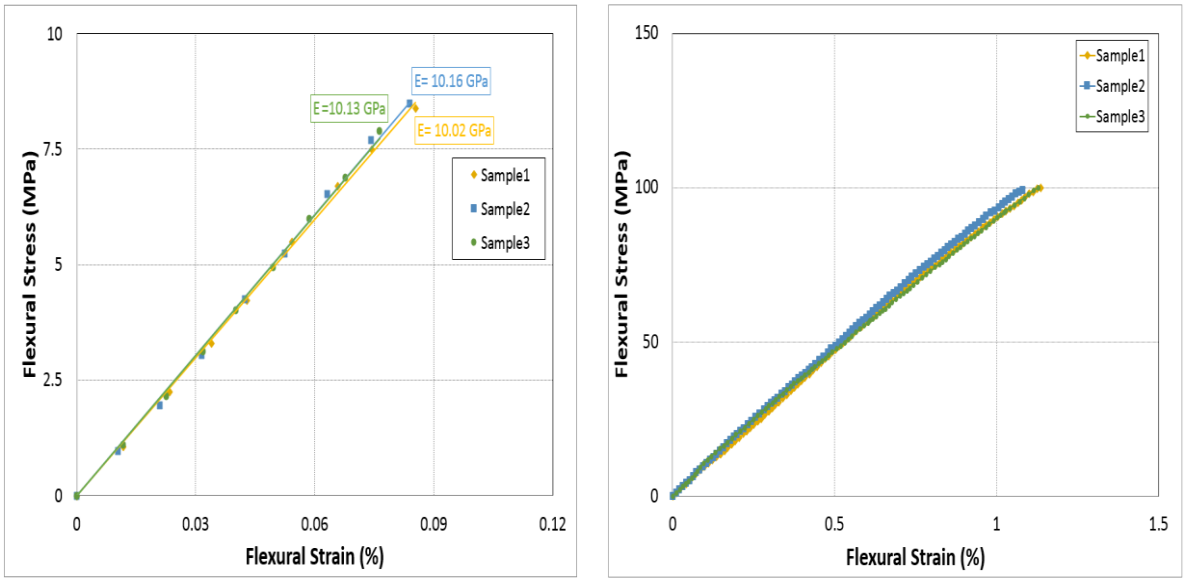

(a) Young's modulus

(b) Overall initial flexural stress-strain behavior

Figure 18: Flexural behavior of all three specimens

The variation in electrical resistance of the CM sensor was gradual with the applied strain during the flexural deflection with good repeatability in results during each cycle, however, the CM sensor in each position showed a distinct change in behavior according to their respective direction according to the roller axis and location between each plie (through-thickness). As discussed before, samples 1 and 2 were tested with sensor A in the top location and aligned with the roller axis to demonstrate the repeatability in the behavior and in-situ monitoring of the CM sensor when prepared in a different batch. CM sensors in all four positions showed a gradual change in their resistance and correlated perfectly with the applied strain, Figure 19. Test 3 was performed to test the position sensitivity of the CM sensor with the loading axis (perpendicular to the specimen) in which sensor A was in the bottom position and the position of the other sensors was changed accordingly Figure 20. CM sensor in all four positions showed a positive change in resistance during the cyclic flexural load with a change in the intensity of the signal with the change of the position in both Cases. However, it was expected to see a negative change in resistance in the place of compressive strain and positive change is resistance in place of tensile strain [12], but this was not seen in the results because of the same reason discussed in section 5.1 i.e. real-time strain monitoring during tensile deformation.

In both cases, the CM sensor in all four positions showed distinct performance which was required to be discussed in detail consecutively to comprehend the detection of deformation during the flexural bending by the CM sensor in each position.

- Sensor A: was in the leg of the star specimen positioned at 0° direction regarding the roller axis and was solitary under the localized compression of the center roller because of the indirect load applied

by the central roller. Sensor A detected minimum strain deformation in case I (positioned on top) while in case II (positioned at the bottom), it detected maximum deformation, Figure 19. This confirmed that the CM sensor was able to detect the tensile elongation in case II but instead of showing the negative change in resistance in case I to detect the compressive strains, it showed a minimum positive change in the resistance which could be because of the densification of the CNT network in the conductive membrane during the curing process of the composite sample and the localized buckling of the fibers. However, changing the position of the CM sensor showed the change in the sensitivity of the sensor with respect to the position and applied load axis, Figure 20.

- Sensor B: was in +45° in case I and in -45° in case II regarding the roller axis while it was situated second from the top in former and second from the bottom in latter case i.e. between ply 2 and 3. In tests 1 and 2, sensor B showed good reproducibility in results and correlated perfectly with the applied strain in each cycle, Figure 19. But, the intensity of the detection signal of sensor B in comparison to sensor A was increased because sensor B was closer to the effect of the indirect localized effect of the central roller in both cases. Comparison of tests 1 and 3 showed that the intensity of the CM sensor signal changed because of the change in the position, Figure 20. As discussed earlier the CM sensor shows good detection of a tensile strain than the compression because the network of CNTs already shows excellent conductance that further compression does not affect its resistance change, Figure 21.

- Sensor C: was in the leg of star specimen along the span length (90° direction), placed between the rollers and between the 3rd and 4th ply. During Case, I, the CM sensor in this position showed maximum intensity in the detection signal and correlated perfectly in each cycle of the applied strain because it was placed in the loaded led and was under the maximum influence of the flexural deflection, Figure 19. Also, in case I (test1 and test 2), it was positioned below the neutral axis of the specimen where the specimen experienced tensile strain and elongation. CM sensor detected showed an increase in resistance with an applied deflection in each cycle and this detection was not localized but along the whole span length. However, in case II when the position of sensor C was a change to above the neutral axis, the intensity of the detection signal dropped because of the higher effect of compression than the tensile deformation, Figure 20. So, even though sensor C was along the span length and under the direct influence of the bending still, its intensity of the signal was less than sensor A and sensor B according to its position in Case II, Figure 21.

- Sensor D: was in the leg positioned at -45° direction and in the bottom position in case I and 45° direction and the top position in case II. It was also not under the direct effect of flexural deflection but only under the. During Case, I (test 1 and test 2), the sensor in position D showed the second-largest intensity in the detection signal after sensor C because of its position in the bottom of the

specimen where it experienced tensile elongation under the indirect localized influence of the central roller, Figure 19. The intensity of the sensor at D position was lower than the sensor in the C position even though maximum strain should be present at the bottom but because sensor C was along the span length in the loaded leg and under the direct influence of flexural bending as discussed before. The comparison of case I and case II showed that the intensity of the signal of the sensor in the D position was decreased remarkably when its position was changed in Case II, Figure 20-21.

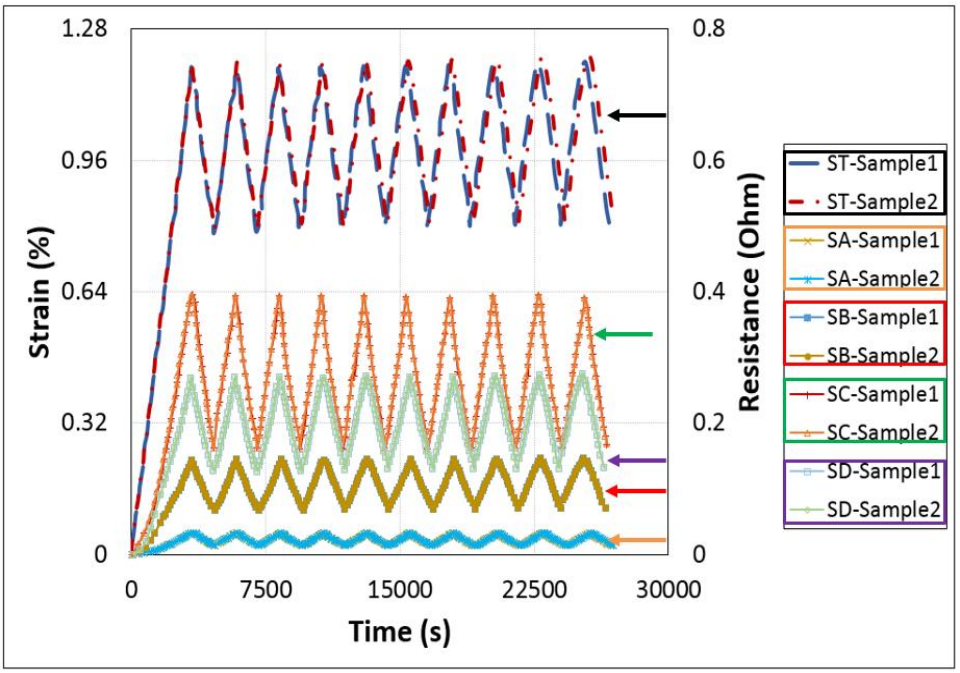

Figure 19: Real-time strain monitoring in composite star specimen during cycle flexural bending using CM sensor

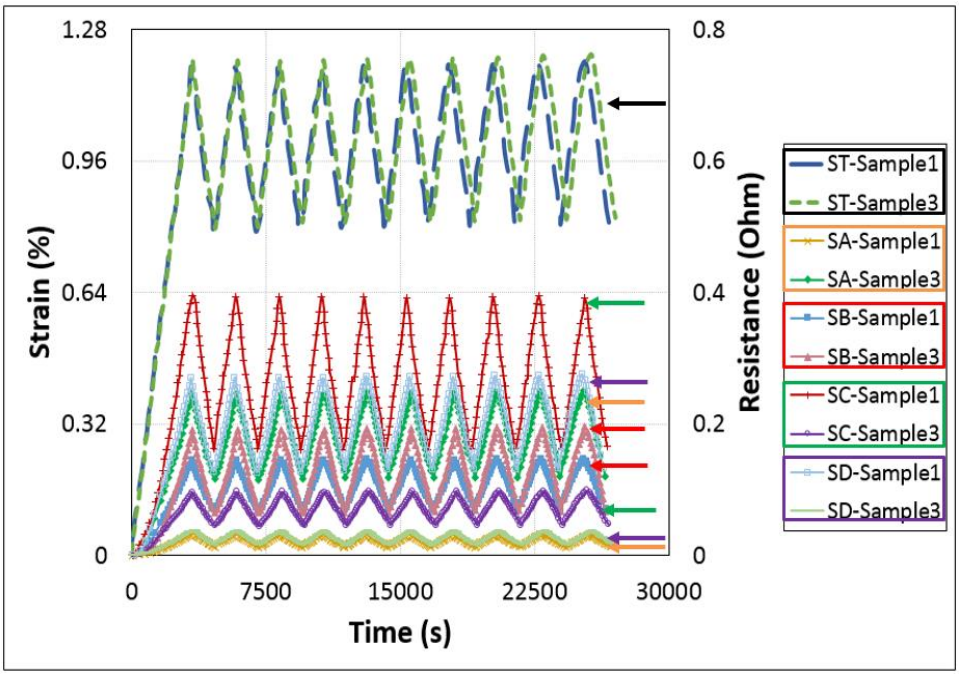

Figure 20: Comparison of real-time strain monitoring in composite star specimen during cycle flexural bending during test 1 (when sensor A is placed in top position according to the loading axis) and test 3 (when sensor A is placed in bottom position according to the loading axis).

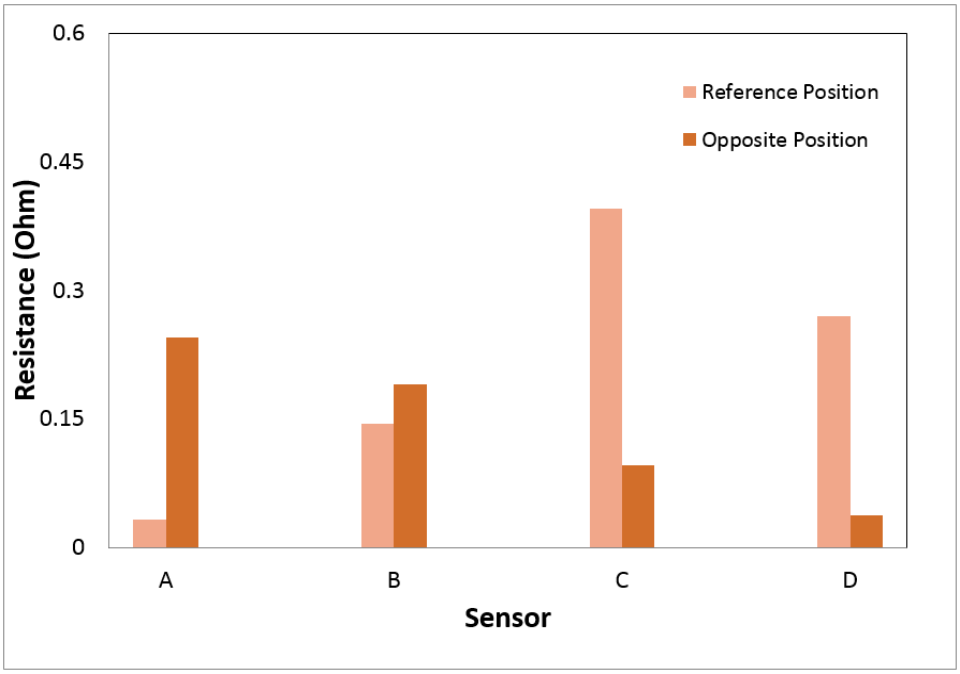

Figure 21: Effect of position and direction on the sensitivity of the CM sensor with respect to the loading axis and position through-thickness.

6 Conclusions

The objective of this extensive experimental study was to develop a conductive membrane consisting

of a CNTs network with high electrical conductance and incorporate it in the composite specimen for real-time strain monitoring applications. This CM sensor showed viable replacement of conventional strain gauges and SHM systems by demonstrating high sensitivity to applied strain in the range of 8-8.25, flexibility 0and 0easy integrated within the composite specimens. The method of placing these sensors in different directions and positions showed that these sensors can detect deformation over large areas and sections of complex structures and in locations that are not normally accessible to conventional methods. The study of real-time monitoring of strain by CM sensor under tensile and flexural cyclic loads demonstrated the influence of the direction with respect to the loading axis on the change in resistance and the influence of the position of the sensor within the plies on the detection signal, respectively. Results confirmed that CM sensors in both tests reacted to the applied stimuli in every direction and showed a distinct change in their change in resistance thus, not only monitoring the deformation but also detecting the amount of damage induced in each position and direction within the composite sample. However, further study is required to understand the precise mechanism responsible for changing the resistance of the sensors to apprehend its response in the transverse direction or under compression strain. Further understanding of these effects on the behavior of CNTs network in the CM sensor could make it possible to tailor the fabrication process of the conductive membrane so that the behavior of the sensor is predictable under both strain deformations i.e. tensile and compression.

References

[1] J. Farringdon, “Wearable electronics and clothing from Philips and Levi,” vol. 10, pp. 22–24, 2001.

[2] F. Axisa, P. M. Schmitt, C. Géhin, G. Delhomme, E. McAdams, and A. Dittmar, “Flexible technologies and smart clothing for citizen medicine, home healthcare, and disease prevention,” *IEEE Trans. Inf. Technol. Biomed.*, vol. 9, pp. 325–336, 2005.

[3] “Universal Serial Fabric Bus, US Army Natick Soldier Systems Center.,” 2013. [Online]. Available: https://www3.natick.army.mil/docs/W911QY-15-R-0016-0001 with Forms.pdf.

[4] C. Simon, E. Potter, M. McCabe, and C. Baggerman, “Smart fabrics technology development,” 2010. [Online]. Available: https://ntrs.nasa.gov/archive/nasa/casi.ntrs.nasa.gov/20100042366.pdf.

[5] K. Diamanti and C. Soutis, “Structural health monitoring techniques for aircraft composite structures,” *Prog. Aerosp. Sci.*, vol. 46, no. 8, pp. 342–352, 2010, doi: https://doi.org/10.1016/j.paerosci.2010.05.001.

[6] A. Ghoshal, M. J. Sundaresan, M. J. Schulz, and P. F. Pai, “Structural health monitoring techniques for wind turbine blades,” *J. Wind Eng. Ind. Aerodyn.*, vol. 85, no. 3, pp. 309–324, 2000, doi: https://doi.org/10.1016/S0167-6105(99)00132-4.

[7] L. C. Hollaway, “A review of the present and future utilisation of FRP composites in the civil infrastructure with reference to their important in-service properties,” *Constr. Build. Mater.*, vol. 24, no. 12, pp. 2419–2445, 2010, doi: https://doi.org/10.1016/j.conbuildmat.2010.04.062.

[8] Y. Qureshi, M. Tarfaoui, K. K. Lafdi, and K. Lafdi, “Development of microscale flexible nylon/Ag strain sensor wire for real-time monitoring and damage detection in composite structures subjected to three-point bend test,” *Compos. Sci. Technol.*, vol. 181, p. 107693, 2019, doi: https://doi.org/10.1016/j.compscitech.2019.107693.

[9] J.-B. Ihn and F.-K. Chang, “Pitch-catch active sensing methods in structural health monitoring for aircraft structures,” *Struct. Heal. Monit.*, vol. 7, no. 1, pp. 5–9, 2008.

[10] Y. Qureshi, M. Tarfaoui, K. K. Lafdi, and K. Lafdi, “Real-time strain monitoring performance of flexible Nylon/Ag conductive fiber,” *Sensors Actuators A Phys.*, vol. 295, pp. 612–622, 2019, doi: https://doi.org/10.1016/j.sna.2019.06.036.

[11] Y. Qureshi, M. Tarfaoui, K. K. Lafdi, and K. Lafdi, “Real-time strain monitoring and damage detection of composites in different directions of the applied load using a microscale flexible Nylon/Ag strain sensor,” *Struct. Heal. Monit.*, vol. 19, no. 3, pp. 885–901, doi: 10.1177/1475921719869986.

[12] Y. Qureshi, M. Tarfaoui, K. K. Lafdi, and K. Lafdi, “In-situ Monitoring, Identification and Quantification of Strain Deformation in Composites under Cyclic Flexural Loading using Nylon/Ag Fiber Sensor,” *IEEE Sens. J.*, p. 1, 2020, doi: 10.1109/JSEN.2020.2969329.

[13] C. Bois, P. Herzog, and C. Hochard, “Monitoring a delamination in a laminated composite beam using in-situ measurements and parametric identification,” *J. Sound Vib.*, vol. 299, no. 4, pp. 786–805, 2007, doi: https://doi.org/10.1016/j.jsv.2006.07.026.

[14] V. Giurgiutiu, A. Zagrai, and J. J. Bao, “Piezoelectric Wafer Embedded Active Sensors for Aging Aircraft Structural Health Monitoring,” *Struct. Heal. Monit.*, vol. 1, no. 1, pp. 41–61, 2002, doi: 10.1177/147592170200100104.

[15] G. Park, H. H. Cudney, and D. J. Inman, “An Integrated Health Monitoring Technique Using Structural Impedance Sensors,” *J. Intell. Mater. Syst. Struct.*, vol. 11, no. 6, pp. 448–455, 2000, doi: 10.1106/QXMV-R3GC-VXXG-W3AQ.

[16] C. C. Ciang, J.-R. Lee, and H.-J. Bang, “Structural health monitoring for a wind turbine system: a review of damage detection methods,” *Meas. Sci. Technol.*, vol. 19, no. 12, p. 122001, Oct. 2008, doi: 10.1088/0957-0233/19/12/122001.

[17] T. G. Gerardi, “Health Monitoring Aircraft,” *J. Intell. Mater. Syst. Struct.*, vol. 1, no. 3, pp. 375–385, 1990, doi: 10.1177/1045389X9000100307.

[18] C. R. Farrar and K. Worden, “An introduction to structural health monitoring,” *Philos. Trans. R. Soc. A Math. Phys. Eng. Sci.*, vol. 365, no. 1851, pp. 303–315, 2007, doi: 10.1098/rsta.2006.1928.

[19] J. Leng and A. Asundi, “Structural health monitoring of smart composite materials by using EFPI and FBG sensors,” *Sensors Actuators A Phys.*, vol. 103, no. 3, pp. 330–340, 2003, doi: https://doi.org/10.1016/S0924-4247(02)00429-6.

[20] W. Staszewski, C. Boller, and G. R. Tomlinson, *Health monitoring of aerospace structures: smart sensor technologies and signal processing*. John Wiley & Sons, 2004.

[21] Y. ZOU, L. TONG, and G. P. STEVEN, “VIBRATION-BASED MODEL-DEPENDENT DAMAGE (DELAMINATION) IDENTIFICATION AND HEALTH MONITORING FOR COMPOSITE STRUCTURES — A REVIEW,” *J. Sound Vib.*, vol. 230, no. 2, pp. 357–378,

2000, doi: https://doi.org/10.1006/jsvi.1999.2624.

[22] A. C. Raghavan and C. Cesnik, “Review of Guided-Wave Structural Health Monitoring,” *Shock Vib. Dig.*, vol. 39, pp. 91–114, 2007, doi: 10.1177/0583102406075428.

[23] S. W. Doebling, C. R. Farrar, M. B. Prime, and D. W. Shevitz, “Damage identification and health monitoring of structural and mechanical systems from changes in their vibration characteristics: A literature review,” doi: 10.2172/249299.

[24] J. P. Andrews, A. N. Palazotto, M. P. DeSimio, and S. E. Olson, “Lamb Wave Propagation in Varying Isothermal Environments,” *Struct. Heal. Monit.*, vol. 7, no. 3, pp. 265–270, 2008, doi: 10.1177/1475921708090564.

[25] N. Muto, H. Yanagida, T. Nakatsuji, M. Sugita, Y. Ohtsuka, and Y. Arai, “Design of intelligent materials with self-diagnosing function for preventing fatal fracture,” *Smart Mater. Struct.*, vol. 1, no. 4, pp. 324–329, Dec. 1992, doi: 10.1088/0964-1726/1/4/007.

[26] X. Wang, S. Wang, and D. D. L. Chung, “Sensing damage in carbon fiber and its polymer-matrix and carbon-matrix composites by electrical resistance measurement,” *J. Mater. Sci.*, vol. 34, no. 11, pp. 2703–2713, 1999, doi: 10.1023/A:1004629505992.

[27] S. Wang and D. D. L. Chung, “Piezoresistivity in continuous carbon fiber polymer-matrix composite,” *Polym. Compos.*, vol. 21, no. 1, pp. 13–19, 2000, doi: 10.1002/pc.10160.

[28] S. Nauman, I. Cristian, F. Boussu, and V. Koncar, “Smart Sensors for Industrial Applications. Part V Piezoresistive, Wireless, and Electrical Sensors,” USA,: K. Iniewski, 2013.

[29] K. S. Karimov, F. A. Khalid, and M. T. S. Chani, “Carbon nanotubes based strain sensors,” *Measurement*, vol. 45, no. 5, pp. 918–921, 2012, doi: https://doi.org/10.1016/j.measurement.2012.02.003.

[30] I. Kang, M. J. Schulz, J. H. Kim, V. Shanov, and D. Shi, “A carbon nanotube strain sensor for structural health monitoring,” *Smart Mater. Struct.*, vol. 15, no. 3, pp. 737–748, Apr. 2006, doi: 10.1088/0964-1726/15/3/009.

[31] E. T. Thostenson and T.-W. Chou, “Real-time in situ sensing of damage evolution in advanced fiber composites using carbon nanotube networks,” *Nanotechnology*, vol. 19, no. 21, p. 215713, Apr. 2008, doi: 10.1088/0957-4484/19/21/215713.

[32] R. J. Grow, Q. Wang, J. Cao, D. Wang, and H. Dai, “Piezoresistance of carbon nanotubes on deformable thin-film membranes,” *Appl. Phys. Lett.*, vol. 86, no. 9, p. 93104, 2005, doi: 10.1063/1.1872221.

[33] Alamusi, N. Hu, H. Fukunaga, S. Atobe, Y. Liu, and J. Li., “Piezoresistive strain sensors made from carbon nanotubes based polymer nanocomposites,” *Sensors*, vol. 11, pp. 10691–10723.

[34] P. Dharap, Z. Li, S. Nagarajaiah, and E. V Barrera, “Nanotube film based on single-wall carbon nanotubes for strain sensing,” *Nanotechnology*, vol. 15, no. 3, pp. 379–382, Jan. 2004, doi: 10.1088/0957-4484/15/3/026.

[35] N. Hu, Y. Karube, C. Yan, Z. Masuda, and H. Fukunaga, “Tunneling effect in a polymer/carbon nanotube nanocomposite strain sensor,” *Acta Mater.*, vol. 56, no. 13, pp. 2929–2936, 2008, doi: https://doi.org/10.1016/j.actamat.2008.02.030.

[36] N. Hu, Y. Karube, M. Arai, T. Watanabe, C. Yan, and Y. Li., “Investigation on sensitivity of polymer/carbon nanotube composite strain sensor.,” *Carbon N. Y.*, vol. 48, no. 680–687, 2010.

[37] B. Hu *et al.*, “Performance characterization of {VGCF}/epoxy nanocomposite sensors under static load cycles and in static structural health monitoring,” *Smart Mater. Struct.*, vol. 22, no. 4, p. 45008, Mar. 2013, doi: 10.1088/0964-1726/22/4/045008.

[38] J. L. Abot *et al.*, “Delamination detection with carbon nanotube thread in self-sensing composite materials,” *Compos. Sci. Technol.*, vol. 70, no. 7, pp. 1113–1119, 2010, doi: https://doi.org/10.1016/j.compscitech.2010.02.022.

[39] S. Iijima, “Helical microtubules of graphitic carbon,” *Nature*, vol. 354, no. 6348, pp. 56–58, 1991, doi: 10.1038/354056a0.

[40] Z. Wan, J. Guo, and M. Jia., “Damage detection of three-dimensional braided composite materials using carbon nanotube thread,” *Sci. Eng. Compos. Mater.*, vol. 24, no. 2, pp. 213-220., 2015.

[41] S. Wang *et al.*, “Smart wearable kevlar-based safeguarding electronic textile with excellent sensing performance.,” *Soft Matter.*, vol. 13, no. 13, pp. 2483–2491, 2017.

[42] Q. Li *et al.*, “Superhydrophobic Electrically Conductive Paper for Ultrasensitive Strain Sensor with Excellent Anticorrosion and Self-Cleaning Property,” *ACS Appl. Mater. Interfaces*, May 2019, doi: 10.1021/acsami.9b03421.

[43] H. Liu *et al.*, “Electrically conductive strain sensing polyurethane nanocomposites with synergistic carbon nanotubes and graphene bifillers,” *Nanoscale*, vol. 8, no. 26, pp. 12977–12989, 2016, doi: 10.1039/C6NR02216B.

[44] D. Kim, J.-E. Bourée, and S. Y. Kim, “Calculation of the field enhancement for a nanotube array and its emission properties,” *J. Appl. Phys.*, vol. 105, no. 8, p. 84315, 2009, doi: 10.1063/1.3091282.

[45] M. Shahi *et al.*, “Effect of purity, edge length, and growth area on field emission of multi-walled carbon nanotube emitter arrays,” *J. Appl. Phys.*, vol. 113, no. 20, p. 204304, 2013, doi: 10.1063/1.4807916.

[46] F. Giubileo *et al.*, “Local probing of the field emission stability of vertically aligned multi-walled carbon nanotubes,” *Carbon N. Y.*, vol. 47, no. 4, pp. 1074–1080, 2009, doi: https://doi.org/10.1016/j.carbon.2008.12.035.

[47] A. Di Bartolomeo *et al.*, “A local field emission study of partially aligned carbon-nanotubes by atomic force microscope probe,” *Carbon N. Y.*, vol. 45, no. 15, pp. 2957–2971, 2007, doi: https://doi.org/10.1016/j.carbon.2007.09.049.

[48] H. Liu, Y. Shi, B. Chen, X. Li, Y. Ding, and B. Lu, “Effect of patterned and aligned carbon nanotubes on field emission properties,” *Vacuum*, vol. 86, no. 7, pp. 933–937, 2012, doi: https://doi.org/10.1016/j.vacuum.2011.07.047.

[49] F. Giubileo *et al.*, “Field emission properties of as-grown multiwalled carbon nanotube films,” *Carbon N. Y.*, vol. 50, no. 1, pp. 163–169, 2012, doi: https://doi.org/10.1016/j.carbon.2011.08.015.

[50] Y. Chen *et al.*, “Emitter spacing effects on field emission properties of laser-treated single-walled carbon nanotube buckypapers,” *Nanotechnology*, vol. 21, no. 49, p. 495702, Nov. 2010, doi: 10.1088/0957-4484/21/49/495702.

[51] P. Rai, D. R. Mohapatra, K. S. Hazra, D. S. Misra, and S. P. Tiwari, “Nanotip formation on a

carbon nanotube pillar array for field emission application," *Appl. Phys. Lett.*, vol. 93, no. 13, p. 131921, 2008, doi: 10.1063/1.2996283.

[52] T.-W. Weng, Y.-H. Lai, and K.-Y. Lee, "Area effect of patterned carbon nanotube bundle on field electron emission characteristics," *Appl. Surf. Sci.*, vol. 254, no. 23, pp. 7755–7758, 2008, doi: https://doi.org/10.1016/j.apsusc.2008.02.020.

[53] R. Seelaboyina, S. Boddepalli, K. Noh, M. Jeon, and W. Choi, "Enhanced field emission from aligned multistage carbon nanotube emitter arrays," *Nanotechnology*, vol. 19, no. 6, p. 65605, Jan. 2008, doi: 10.1088/0957-4484/19/6/065605.

[54] S. Roy *et al.*, "Enhanced Field Emission and Improved Supercapacitor Obtained from Plasma-Modified Bucky Paper," *Small*, vol. 7, no. 5, pp. 688–693, 2011, doi: 10.1002/smll.201002330.

[55] M. Kaempgen, C. K. Chan, J. Ma, Y. Cui, and G. Gruner, "Printable Thin Film Supercapacitors Using Single-Walled Carbon Nanotubes," *Nano Lett.*, vol. 9, no. 5, pp. 1872–1876, May 2009, doi: 10.1021/nl8038579.

[56] A. Bonanni, M. J. Esplandiu, and M. del Valle, "Impedimetric genosensors employing COOH-modified carbon nanotube screen-printed electrodes," *Biosens. Bioelectron.*, vol. 24, no. 9, pp. 2885–2891, 2009, doi: https://doi.org/10.1016/j.bios.2009.02.023.

[57] N. Behabtu, M. J. Green, and M. Pasquali, "Carbon nanotube-based neat fibers," *Nano Today*, vol. 3, no. 5, pp. 24–34, 2008, doi: https://doi.org/10.1016/S1748-0132(08)70062-8.

[58] R. H. Baughman *et al.*, "Carbon Nanotube Actuators," *Science (80-.).*, vol. 284, no. 5418, pp. 1340–1344, 1999, doi: 10.1126/science.284.5418.1340.

[59] J. Sebastian *et al.*, "Health monitoring of structural composites with embedded carbon nanotube coated glass fiber sensors," *Carbon N. Y.*, vol. 66, pp. 191–200, 2014, doi: https://doi.org/10.1016/j.carbon.2013.08.058.